Soft Matter

PAPER

Cite this: *Soft Matter*, 2016, 12, 8958

Contact-line pinning controls how quickly colloidal particles equilibrate with liquid interfaces

Anna Wang,[a] Ryan McGorty,†[b] David M. Kaz‡[b] and Vinothan N. Manoharan*[ab]

Received 24th July 2016,
Accepted 5th October 2016

DOI: 10.1039/c6sm01690a

www.rsc.org/softmatter

Previous experiments have shown that spherical colloidal particles relax to equilibrium slowly after they adsorb to a liquid–liquid interface, despite the large interfacial energy gradient driving the adsorption. The slow relaxation has been explained in terms of transient pinning and depinning of the contact line on the surface of the particles. However, the nature of the pinning sites has not been investigated in detail. We use digital holographic microscopy to track a variety of colloidal spheres—inorganic and organic, charge-stabilized and sterically stabilized, aqueous and non-aqueous—as they breach liquid interfaces. We find that nearly all of these particles relax logarithmically in time over timescales much larger than those expected from viscous dissipation alone. By comparing our results to theoretical models of the pinning dynamics, we infer the area per defect to be on the order of a few square nanometers for each of the colloids we examine, whereas the energy per defect can vary from a few kT for non-aqueous and inorganic spheres to tens of kT for aqueous polymer particles. The results suggest that the likely pinning sites are topographical features inherent to colloidal particles—surface roughness in the case of silica particles and grafted polymer "hairs" in the case of polymer particles. We conclude that the slow relaxation must be taken into account in experiments and applications, such as Pickering emulsions, that involve colloids attaching to interfaces. The effect is particularly important for aqueous polymer particles, which pin the contact line strongly.

1 Introduction

The strong binding of colloidal particles to interfaces is exploited in a range of applications. Particles can stabilize oil–water interfaces in Pickering emulsions,[1] which are used in food,[2,3] oil recovery,[4] pharmaceuticals, and cosmetics.[5] Oil–water interfaces can also be used to scaffold the assembly of particles into colloidosomes,[6] Janus particles,[7] monolayers,[8] and photolithography masks.[9] Because the driving force for adsorption is large—the adsorption of a single particle reduces the interfacial energy of the system by many times the thermal energy kT—it is sometimes (and often tacitly) assumed that such particles reach their equilibrium contact angle rapidly once they breach the interface. Indeed, if viscous drag were the only force opposing the interfacial energy gradient, particles would relax to equilibrium exponentially with a time constant on the order of a microsecond.[10]

However, when Kaz, McGorty, and coworkers[11] directly measured the adsorption dynamics of polystyrene microspheres at an interface between water/glycerol and oil, they found that the particles relaxed toward equilibrium logarithmically, not exponentially. Furthermore, the relaxation was so slow that the time projected for the particles to reach the equilibrium contact angle of 110° was months to years—far longer than typical experimental timescales. Later, Coertjens and coworkers[12] directly imaged polymer particles at vitrified interfaces and found that the average contact angle increased an hour after adsorption. Kaz *et al.* proposed that the slow relaxation is due to pinning and unpinning of the contact line on nanoscale heterogeneities ("defects") on the particle surfaces. The pinning and unpinning events contribute to a larger dissipation of energy than viscosity alone. Using a model of contact-line hopping based on molecular-kinetic theory (described in the Background section below), they were able to infer the sizes of the defects.

More recent work has elucidated and expanded on how contact line pinning affects the dynamics of particles at interfaces. Colosqui and coworkers[10] developed a model based on Kramer's theory for the full equilibrium dynamics of the particles, including not only the logarithmic regime, but also the dynamics shortly after the breach and close to equilibrium. As we describe below in the Background section, this model can be fit to experimental data to estimate the pinning energy per defect. Other work examines the effect of pinning on particle dynamics lateral to an interface. Recent experimental studies by Boniello *et al.*[13] indicate

[a] *Harvard John A. Paulson School of Engineering and Applied Sciences, Harvard University, Cambridge, MA 02138, USA. E-mail: vnm@seas.harvard.edu*
[b] *Department of Physics, Harvard University, Cambridge, MA 02138, USA*
† Present address: Department of Physics and Biophysics, University of San Diego, San Diego, CA 92110, USA.
‡ Present address: Agilent Technologies, Santa Clara, CA 95051, USA.

that the lateral diffusion of colloidal particles at a fluid interface is likely slowed by transient pinning events. Sharifi-Mood and coworkers[14] showed that strong pinning can locally distort the interface around a colloidal particle, affecting how particles migrate on a curved surface.

These studies highlight the importance of contact-line pinning for understanding the dynamics of colloids at interfaces. The observed slow relaxation has direct consequences for the applications we list above: in a collection of identical particles at an interface, such as the surface of a Pickering emulsion droplet, the particles can have different contact angles that change over time. Because the contact angle of a particle determines the length of the three-phase contact line and how much of the particle is exposed to the aqueous or oil phases, it affects the capillary[15] and electrostatic interactions between particles.[16] Contact angles that change over time might help explain the heterogeneous pair-interactions[17,18] and long-ranged attractions observed between identically charged particles.[19] For the particular case of Pickering emulsions, the emulsion type (water-in-oil, or oil-in-water) also depends on the contact angle,[20] and so a changing contact angle might change the emulsion type and stability over time.

Here we focus on understanding how ubiquitous the pinning is and what causes it. To do this, we follow the approach of Kaz *et al.*[11] and Wang *et al.*[21] and use digital holographic microscopy, a fast three-dimensional imaging technique, to measure the motion of spherical particles as they breach liquid interfaces. However, here we examine a much wider variety of particles and surface functionalities. We find that charge-stabilized polymer spheres (including a variety of emulsion-polymerized particles), surfactant-stabilized polymer spheres, and large (several micrometers in diameter) silica spheres all relax logarithmically to equilibrium, though some systems, including oil-dispersed PMMA particles and smaller silica spheres, reach equilibrium on experimental timescales. By fitting models to the data, we are able to extract details about the pinning sites. For example, we find that the heterogeneities on aqueous-dispersed polymer particles pin the contact-line with an order of magnitude more energy than those on other particles, resulting in a longer logarithmic regime. We conclude that the likely pinning sites are nanoscale topographical features such as polymer "hairs."

2 Background

In this section we describe the theories that have been developed to explain the slow relaxation of colloidal particles at interfaces, and how fitting them to experimental data reveals details of the pinning dynamics. The logarithmic trajectories observed by Kaz *et al.*[11] can be explained by using molecular kinetic theory (MKT) to model the motion of the contact line as a dynamic wetting process.[22] In this model, as the contact line moves across the surface of the particle, it encounters defects of area A that each pin it with energy ΔU. The contact line requires a thermal "kick" to keep it moving toward equilibrium: once it unpins from one defect, it can then move along the particle until it gets caught on another defect. The characteristic length the contact line traverses before reaching another defect is $\ell = A/p$,[10] where p is the perimeter of the contact line. This model explains why the particle motion appears continuous in the experiments: in practice, ℓ is on order of picometers,[10] much smaller than displacements that we can measure. The model also explains why the particle slows as it progresses through the interface: the driving force decreases as the particle gets closer to equilibrium, while the pinning energy and the density of defects remain the same (Fig. 1).

The activated hopping of the contact line results in much more dissipation than that predicted from hydrodynamics. If hydrodynamics were the only relevant effect, we would expect the particle to follow an exponential path to equilibrium with a timescale $T_D \approx \eta r/\sigma_{ow}$, where η is a weighted average of the viscosities of the two fluids, r the radius of the particle, and σ_{ow} the interfacial tension between oil and water.[10] For a 1 μm-radius particle at a water–alkane interface, T_D is approximately 0.1 μs, which is several orders of magnitude smaller than the times observed in experiments.[11]

A model based on MKT, presented in the ESI section of Kaz *et al.*,[11] captured the experimentally observed dynamics from 10^{-2}–10^{2} s after the breach—the point where the particle first comes into contact with the interface and a three-phase contact line is formed. This model is not valid for shorter times, where the length of the contact line rapidly increases; instead, it is intended to model the behavior in the logarithmic regime, where the contact line perimeter changes slowly with time. By fitting the model to the data, the authors inferred that the area per pinning defect was on the order of a few square nanometers. This value is larger than the molecular scales the theory was derived for, but there are other successful applications of MKT to surfaces with defects larger than 1 nm^2.[23,24]

To show how the area per defect affects the dynamics, we present a brief derivation of the model from Kaz *et al.*[11] We model the activated hopping process using an Arrhenius equation for the velocity of the contact line.[22] Far from equilibrium,

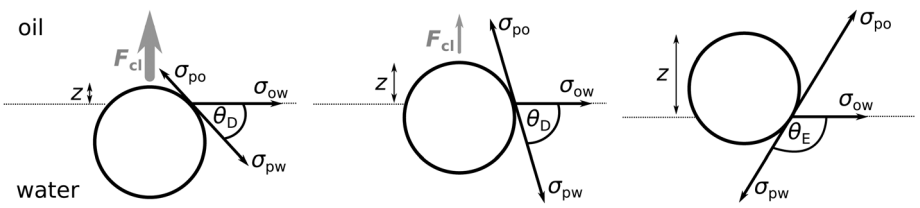

Fig. 1 When the particle first breaches the interface, the unbalanced interfacial tensions cause the particle to move. This unbalanced force decreases as the particle approaches equilibrium, where the dynamic contact angle θ_D reaches its equilibrium value θ_E and the force F_{cl} goes to zero.

we can neglect backward hops. In this case, the velocity of the contact line tangent to the particle is given by

$$V = V_0 \exp\left(-\frac{\Delta U}{kT} + \frac{F_{cl}(t)A}{2kT}\right) \quad (1)$$

where V_0 is a molecular velocity scale, and kT is the thermal energy. The force per unit length on the contact line, F_{cl}, is determined by the tangential component of the oil–water (σ_{ow}), particle–oil (σ_{po}), and particle–water (σ_{pw}) interfacial tensions (Fig. 1):

$$F_{cl} = \sigma_{ow}\cos\theta_D(t) + \sigma_{pw} - \sigma_{po} = \sigma_{ow}(\cos\theta_D(t) - \cos\theta_E) \quad (2)$$

where θ_D is the dynamic contact angle.

Substituting eqn (2) into (1) and rewriting the resulting equation of motion in terms of the observable axial coordinate z, we obtain

$$\dot{z} = \nu r\sin(\theta_D)\exp\left(\frac{A\sigma_{ow}z}{2rkT}\right) = \nu\sqrt{z(2r-z)}\exp\left(\frac{A\sigma_{ow}z}{2rkT}\right) \quad (3)$$

where r is the radius of the particle and

$$\nu = (V_0/r)\exp(-\Delta U/kT + (1 - \cos\theta_E)A\sigma_{ow}/2kT).$$

In deriving eqn (3) we have assumed that the interface remains flat at all times. We have also let $z = 0$ when the particle first touches the interface (at $\theta_D = 0$), from which we obtain $z = r(1 - \cos\theta_D)$ and $V = r\dot{\theta}_D = \dot{z}/\sin\theta_D$.

When the particle is close to equilibrium, we can expand around the equilibrium contact angle and solve the resulting differential equation to obtain the equation of motion

$$z \approx \frac{2rkT}{A\sigma_{ow}}\log\left(\frac{A\sigma_{ow}}{2rkT}\nu r(\sin\theta_E)t\right)$$

which we can rewrite as

$$\frac{z}{r} \approx \frac{2kT}{A\sigma_{ow}}\log\frac{t}{t_0} + C; \quad C = \frac{2kT}{A\sigma_{ow}}\log\left(\frac{A\sigma_{ow}}{2rkT}\nu r(\sin\theta_E)t_0\right). \quad (4)$$

Eqn (4) shows that the trajectory of the particle is approximately logarithmic in time. We can infer the area per defect A from the slope of a plot of z as a function of $\log t$. We cannot determine the constant C—and hence the pinning energy per defect ΔU, which is embedded in ν—by fitting this model to the data. We therefore choose an arbitrary t_0 ($t_0 = 1$ s).

To determine the pinning energy per defect, ΔU, we must observe where the logarithmic regime begins. Colosqui *et al.*,[10] using Kramer's theory,[25] showed that particles having heterogeneous surface defects initially relax exponentially and then logarithmically. The models from Kaz *et al.* and Colosqui *et al.* are mathematically equivalent[10] when the dynamic contact angle θ_D is approximately $\pi/2$. The area per defect A from Kaz *et al.* is related to the length scale l from Colosqui *et al.* by $A \sim 2\pi R^* l$, where R^* is the radius of the contact line when the particle is at z_C, and z_C is the height at which the relaxation changes from exponential to logarithmic. The crossover point between exponential and logarithmic regimes can be used to infer ΔU, if the equilibrium height of the particle z_E is known or can be estimated:

$$z_E - z_C = \frac{\Delta U\pi R^*}{2\sigma_{ow}A}. \quad (5)$$

To analyze our experimental data we fit eqn (4) to the logarithmic regime to obtain A and then use eqn (5) to determine the defect energy ΔU. We note that these models capture only the gross features of the trajectories. A more recent model[26] expands on the model of Colosqui *et al.* to include extra dissipative effects. This model captures both the short- and long-time behavior of the experimental results from Kaz *et al.* well. Here, because we are interested primarily in the two parameters A and ΔU, we do not seek to capture the full time-dependence of the adsorption process, and we examine our results in the context of the simpler models from Kaz *et al.* and Colosqui *et al.*

3 Materials and methods

3.1 Particles and interfaces

To determine what kinds of surface features affect how a particle relaxes to equilibrium, we track particles with a variety of different surface properties as they breach an interface between an aqueous phase and oil. The types of particles we examine are listed in Table 1. They include 1.9 μm-diameter charge-stabilized sulfate- and carboxyl-functionalized polystyrene (PS, Invitrogen), 2.48 μm-diameter sulfate-functionalized poly(methyl methacrylate) (PMMA, Bangs Laboratories, synthesized by emulsion polymerization), 1.7 μm-diameter polyvinylalcohol-stabilized PS (synthesized according to the procedure in Paine *et al.*[27]), 3.7 μm-diameter polyvinylpyrrolidone-stabilized PMMA (synthesized according to the procedure in Cao *et al.*[28]), and 1.0 μm-diameter bare silica microspheres with SiOH surface groups (Bangs Laboratories). We centrifuge and wash each suspension ten times in deionized water (EMD Millipore, resistivity = 18.2 MΩ cm) to remove contaminants and surface-active compounds, then dilute them for use in experiments.

Table 1 Particles used in breaching experiments, along with the shortened name we use to refer to them in the text

Name	Particle	Phase	Diameter (μm)
PMMA	Sulfate-functionalized PMMA	Aqueous	2.48
PVP-PMMA	Polyvinylpyrrolidone-stabilized PMMA	Aqueous	3.67
Sulfate-PS	Sulfate-functionalized PS	Aqueous	1.88
Carboxyl-PS	Carboxylate-functionalized PS	Aqueous	1.88
PVA-PS	Polyvinylalcohol-stabilized PS	Aqueous	1.65
PDMS-PMMA	Polydimethylsiloxane-stabilized PMMA	Oil	1.1
PHSA-PMMA	Poly(12-hydroxystearic acid)-stabilized PMMA	Oil	1.6
Silica	Bare silica	Aqueous or oil	1.0
Large silica	Bare silica	Oil	4.0

Table 2 Aqueous phase-decane interfaces used, along with the names we use to refer to them

Name	Aqueous phase (index)	Oil (index)
Water/glycerol	59% w/w glycerol in water (1.411)	Decane (1.411)
Water	Water (1.333)	Decane (1.411)
Water/ethanol	10% v/v ethanol in water (1.380)	Decane (1.411)

We also examine several different types of oil-dispersible particles: 1.0 μm-diameter (Bangs Laboratories) and 4.0 μm-diameter (AngstromSphere) silica microspheres, both with SiOH surface groups, 1.1 μm-diameter polydimethylsiloxane-stabilized PMMA (synthesized according to the procedure in Klein *et al.*[29]), and 1.6 μm-diameter poly(12-hydroxystearic acid)-stabilized PMMA particles (synthesized according to the procedure in Elsesser *et al.*[30]). We wash the particles five times in decane (≥99%, anhydrous, Sigma-Aldrich) to remove possible contaminants. We discard any macroscopic colloidal aggregates and keep the freely suspended particles for experiments.

We prepare different aqueous phases from deionized water, anhydrous glycerol (≥99%, Sigma-Aldrich), pure ethanol (100%, KOPTEC), and hydrochloric acid (Fluka). All of the aqueous solutions contain 100 mM NaCl (99.5%, EMD) to screen any electrostatic repulsion between the particle and the interface.[11] For the oil phase we use decane (≥99%, anhydrous, Sigma-Aldrich) which is first filtered through a PTFE membrane filter (Acrodisc). The different liquid–liquid interfaces we use in experiments are summarized in Table 2.

We measure the interfacial tension between water/glycerol and decane using the pendant drop method.[31,32] A 1 mL syringe (Sigma-Aldrich) with a blunt end syringe needle (18 gauge, Kimble) is filled with the aqueous phase. The needle is then submerged into a disposable cuvette (VWR) filled with decane. A droplet of the aqueous phase is slowly injected into decane while images are recorded. The profile of the droplet is analyzed from the images to determine the interfacial tension.

3.2 Sample preparation

Our custom-made polyether ether ketone (PEEK) sample cells are glued to a glass coverslip with UV-cured epoxy (Norland 60). A detailed description of their fabrication can be found in the ESI of Kaz *et al.*[11] Using these cells, we create a stable oil–water interface consisting of a 30–80 μm-thick aqueous phase and a 2–3 μm-thick decane superphase. We use No. 1 coverslips (VWR) so that the interface is within the working distance of an oil-immersion objective (NA = 1.4, Nikon CFI Plan Apo VC 100×) or water-immersion objective (NA = 1.2, Nikon CFI Plan Apo VC 60×). We bake all glassware used to handle the colloidal particles and fluids in a pyrolysis oven (Pyro-Clean Tempyrox) to incinerate organics, then sonicate and wash the glassware with deionized water. This protocol is designed to eliminate interfacially-active contaminants.

We place the sample cell on a Nikon TE-2000 inverted microscope. We focus 5–15 μm below the interface to capture holograms of individual particles as they breach. If we start with particles that are suspended in the aqueous phase, we push them toward the interface using radiation pressure (force less than 1 pN) from out-of-focus optical tweezers, as shown in Fig. 2. If the particles are suspended in oil, we simply allow them to sediment toward the interface.

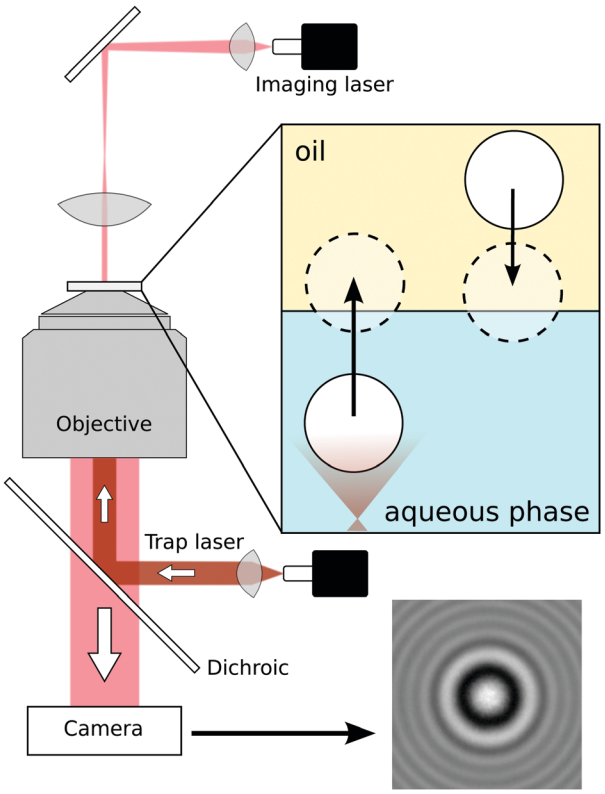

Fig. 2 Experimental setup. The sample sits on an inverted microscope and is illuminated from above with a collimated 660 nm laser. The hologram formed by the interference of the scattered light from the sample with the undiffracted beam is then captured on a camera. We push spheres from the aqueous phase toward the interface with an 830 nm laser. To observe the breaching and relaxation of a particle from the aqueous phase, we push it gently toward the interface using optical tweezers, and measure its trajectory using holographic microscopy. To observe particles breaching from the oil phase, we simply let the particles fall to the interface.

3.3 Tracking particles with digital holographic microscopy

We use an in-line digital holographic microscope, based on a modified Nikon TE-2000 inverted microscope, to track the particles with high temporal and spatial resolution in all three dimensions (Fig. 2). We illuminate samples with a 660 nm imaging laser (Opnext HL6545MG) that is spatially filtered through a single-mode optical fiber (OzOptics SMJ-3U3U-633-4/125-3-5) and collimated. We use a counter propagating 830 nm trap laser (Sanyo DL8142-201), which is spatially filtered through a single-mode optical fiber (OzOptics SMJ-3U3U-780-5/125-3-5), to push particles toward the interface.

The imaging beam (typically 50 mW power) scatters from the sample and interferes with undiffracted light to produce an interference pattern, or hologram. After passing through the objective, holograms are recorded on a monochrome CMOS camera (Photon Focus MVD-1024E-160-CL-12), captured with a frame grabber (EPIX PIXCI E4), and then saved to disk for further processing. We use a short camera exposure time, 20 μs,

to minimize motion blur, and we capture holograms at up to 2000 frames per second, giving us sub-millisecond time resolution. A background image, taken in a part of the sample with no particles, is also recorded and divided from each time-series of holograms to remove artifacts arising from scattering from imperfections on the camera, lenses, and mirrors.

The background-divided holograms are analyzed using our open-source software package HoloPy (http://manoharan.seas.harvard.edu/holopy). To extract the particle trajectories, we fit the Lorenz–Mie scattering model to each background-divided hologram, as described in Fung *et al.*,[33] following the work of Ovryn and Izen[34] and of Lee and coworkers.[35]

The accuracy of the Lorenz–Mie model depends on the refractive index mismatch between the two liquid phases. The Lorenz–Mie scattering solution used to analyze the holograms is exact only for particles in an optically homogeneous medium. Exact light scattering solutions for particles straddling an optically discontinuous boundary do not exist. Therefore, to determine the position of bound particles with maximum accuracy, we index-match the aqueous phase to decane (n = 1.41) by mixing anhydrous glycerol ($\geq$99%, Sigma-Aldrich) with water to make a solution of 59% w/w glycerol so that the system is optically continuous. This index-matching also eliminates reflections from the fluid–fluid interface, which would produce additional interference.

For some of the experiments, we cannot index match the aqueous medium to the oil phase. Because silica particles typically have a refractive index of 1.42 at our imaging wavelength (660 nm) and a high density compared to water, we cannot obtain sufficient radiation pressure to push them toward the interface if they are submerged in an aqueous medium with n = 1.41. Instead, we disperse them in water (n = 1.33) so that the refractive index contrast between the particles and medium is large enough for us to manipulate them with the trapping laser. In our analysis, we allow the refractive index of the particle relative to that of the medium to vary during the fit, which helps compensate for the change in medium index as the particle moves through the interface. In this way we are able to measure the approximate relaxation behavior of the silica spheres.

Because microscope objectives and their immersion fluids are designed to image objects in two dimensions, a difference in refractive index between the immersion oil and the medium leads to spherical aberration, which distorts distances in the axial direction[36] and compromises the positioning accuracy. To mitigate this effect, we use an immersion oil with n = 1.4140 (Series AA, Cargille) with our 100× oil-immersion objective for samples where we index-match the aqueous phase to decane (n = 1.41). In experiments where pure water (n = 1.33) is the aqueous phase, we use a water-immersion objective with water as the immersion fluid.

4 Results

4.1 Slow relaxation is not particular to a water/glycerol–decane interface

We begin by showing that the slow relaxation of particles at an interface is not particular to the decane–water/glycerol system of Kaz *et al.*[11] In that work, the aqueous phase was designed to match the refractive index of decane yet retain an interfacial tension and Debye screening length similar to water. Here we track sulfate-PS particles as they approach interfaces from different aqueous solutions (Table 2).

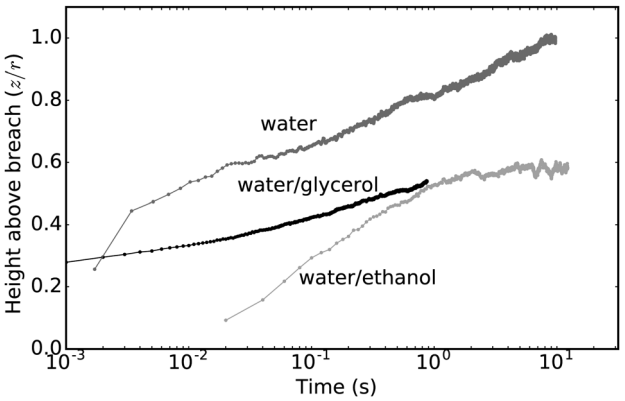

Fig. 3 Typical trajectories of sulfate-PS particles as they breach various aqueous phase-oil interfaces, as listed in Table 2. The distance between the top surface of the particle and the interface is shown as a function of the time after the breach. All of the trajectories show logarithmic relaxation. We define z = 0 μm as the height at which the particle and interface first touch.

The motion of the polystyrene particles through the interface is approximately logarithmic with time in all of the systems, as shown in Fig. 3. We note that the different starting times for the plots are an artifact of the logarithmic time-axis and the different frame rates used to acquire the data. The differences in slopes for the trajectories are due in part to the different refractive-index mismatches (and hence tracking errors) in the three systems, and in part to the different interfacial tensions and dielectric constants in the systems. However, we do not expect any of these effects to change the functional (logarithmic) relationship between height and time. Therefore, we conclude that the slow dynamics are not unique to the water/glycerol and decane system studied in Kaz *et al.*[11] and are potentially relevant to a variety of other liquids.

4.2 Topographical features on polymer particles pin the contact line

Though colloidal particles may appear smooth under optical and even scanning electron microscopy, the particle surfaces contain nanoscale heterogeneities such as charges, asperities and, in the case of polymer particles, polymer "hairs."[37,38] To determine which of these features is responsible for the slow relaxation, we return to the index-matched water/glycerol and decane system and quantitatively measure how particles with different surface features breach the interface. From the trajectories we determine the area per defect, A, by fitting eqn (4) to the logarithmic regime of the measured trajectories. Kaz and coworkers found that A was on the order of the area per charge group for sulfate- ($A \approx 5$ nm^2), carboxyl- ($A \approx 3$ nm^2), amidine- ($A \approx 15$ nm^2), and carboxylate-modified-latex ($A \approx 25$ nm^2) spheres. These results suggest that the charges themselves,

Table 3 Zeta potentials of PS-carboxyl latex at different acid concentrations

Concentration of HCl (M)	Zeta potential (mV)
0	-95 ± 10
10^{-5}	-68 ± 2
10^{-4}	-60 ± 2
10^{-3}	-24 ± 1

or some surface features associated with the charges, could be the pinning sites.

To understand if and how the charges influence the pinning, we do experiments on PS-carboxyl spheres suspended in a 59% glycerol in water solution containing 100 mM NaCl. We work with carboxyl-functionalized spheres because the pK_a is higher than that of sulfate-functionalized spheres, so that the charge can be adjusted by changing the pH over a moderate range. We add acid to the suspensions and measure the zeta potentials of the particles using a Beckman Coulter DelsaNano C zeta potentiometer. The zeta potential decreases by a factor of about four over a range of acid concentrations from 0 to 10^{-3} M (Table 3). Measurements of the interfacial tension using the pendant drop method with a slight index mismatch, caused by increasing the water content in the aqueous phase by about 1% w/w, confirm that the interfacial tension does not vary with acid concentration.

We find that at any given time after the particles breach, particles submerged in higher acid concentrations are at larger heights (Fig. 4). There are two possible interpretations of this observation in the context of Kramer's theory and eqn (5): either the energy of the defect decreases with acid concentration, or the equilibrium contact angle increases with acid concentration. These two quantities cannot be determined independently using either of the two dynamic models;[10,11] however, it stands to reason that a smaller surface charge should increase the hydrophobicity of the particles and thus their equilibrium contact angle.

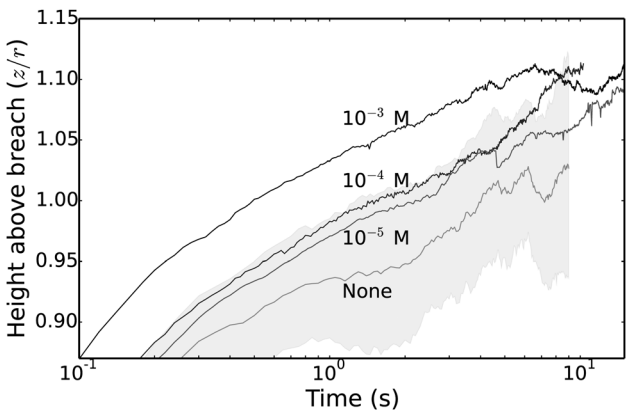

Fig. 4 Trajectories of carboxyl-functionalized latex particles in solutions of varying acid concentration (HCl concentrations are marked above each curve). Lines are the average of five particle trajectories at each concentration. The gray shaded region shows the uncertainty in the zero-HCl-concentration measurement, as determined by the standard deviation on the five trajectories. It is representative of the uncertainties at the other concentrations.

To better understand the nature of the pinning sites, we fit eqn (4) to the logarithmic regime in our data (Fig. 4). The area per defect, which influences the slope of the trajectory, is between 4 nm^2 and 6 nm^2 for each of the four samples. The areas per defect measured here and in Kaz *et al.*[11] differ by orders of magnitude from the roughly (100 nm)^2 chemical heterogeneities of polystyrene particles measured under atomic force microscopy.[39] This disparity suggests that the defects are not the chemical patches that are seen under surface characterization. Moreover, the fact that the areas per defect are nearly constant, despite the large variation in zeta potential (and hence area per charge) with acid concentration, suggests that the pinning sites are not the charges themselves but rather topographical features associated with the charged groups.

Prompted by a question from a reviewer of this manuscript, we also consider whether the slow relaxation might be related to swelling of the particles and subsequent deformation, as discussed by Park *et al.*[40] and Tanaka *et al.*[41]. To determine whether the particles swell as they come into contact with decane, we measure the refractive index of our particles throughout the whole trajectory. If the polystyrene particles were swelling upon contact with decane, we would expect their refractive index to decrease, since n_{PS} is 1.59, while n_{decane} is 1.41. However, we find $n = 1.593 \pm 0.001$ before the breach and $n = 1.590 \pm 0.002$ several seconds after the breach (where the error is the standard error from fitting individual time points in a series). We conclude that there is no significant swelling during the breaching process.

We probe the breaching behavior of a range of other polymer particles to gain further insights. We examine both charge-stabilized and sterically-stabilized particles. The charge-stabilized particles include sulfate-PS and PMMA, both of which are synthesized by emulsion polymerization, while the sterically-stabilized particles include PVA-PS and PVP-PMMA, both of which are synthesized by dispersion polymerization (Table 1).

All of these polymer particles relax logarithmically after breaching, as shown in Fig. 5. We fit eqn (4) to the data to yield $A = 4.6$–11 nm^2 for the particles. Using eqn (5), we calculate the

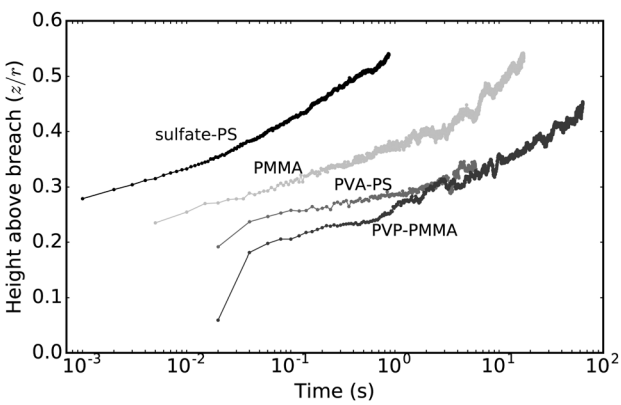

Fig. 5 Typical trajectories of different polymer particles as they breach interfaces between water/glycerol and decane. The particle details are listed in Table 1. The height of the particle above the interface as a function of the time after the breach is shown. All the trajectories show logarithmic relaxation.

pinning energies using σ_{ow} = 37 mN m^{-1}, T = 295 K, and, for sulfate-PS, an equilibrium contact angle of 116° ± 10°[42,43] and z_C/r = 0.3; for PVA-PS, an equilibrium contact angle of 100° ± 20°§ and z_C/r = 0.2; and, for both types of water-dispersed PMMA particles, an equilibrium contact angle of 90° ± 30°¶ and z_C/r = 0.2. We find that ΔU = 50–100 kT, as shown in Table 4.

We also examine the relaxation of PDMS-PMMA and PHSA-PMMA particles, both of which are sterically stabilized and dispersed in the oil phase. We can determine the contact angle of the particles (see Fig. 6) from the heights before and after they breach the interface. Both PHSA- and PDMS-stabilized particles reach a steady-state contact angle of 130–150° within a second of breaching. We find the steady-state contact angle is 135° ± 10° for the PDMS-stabilized particles, and 150° ± 5° for the PHSA-stabilized particles, where the uncertainty is determined from the standard error in the measurement of the height for five different particles. These contact angles are close to the those measured for PMMA particles at a water–decane interface using the freeze-fracture shadow-casting cryoSEM technique (130° ± 12°) and using the gel-trapping technique (157° ± 6°).[43,44]

The relaxation of the sterically stabilized PMMA particles is much faster than that of polymer spheres dispersed in the aqueous phase. To understand this difference, we use the two dynamical models to infer the area and pinning energy per defect. Fitting eqn (4) to the first second of the breaching trajectory for the PDMS-PMMA particle (Fig. 6c) yields A = 8 nm^2. From eqn (5), we calculate the pinning energy using z_C/r = 0.16, σ_{ow} = 37 mN m^{-1}, T = 295 K and R^* = 330 nm. We find ΔU = 4 kT. Thus the area per defect is comparable to that of the aqueous-dispersed particles, but the energy per defect is an order of magnitude smaller.

Because these particles likely have few charges, the area per defect is too small to be comparable to the area per charged group. So in this case, too, the evidence points to topographic features as the pinning sites. In the Discussion section we revisit the question of why the pinning energy is so much larger for the aqueous particles than the oil-dispersed ones. First, however, we examine the nature of the pinning sites on inorganic particles.

4.3 Inorganic particles can also pin contact lines

We find that large, 4 μm bare silica spheres approaching a water/glycerol interface from the decane phase relax logarithmically after breaching but reach a steady-state height after less than 1 s (Fig. 7). These silica particles are large enough that the slow evolution of the fringe pattern can be detected by eye, as shown in the insets in Fig. 7. Fitting eqn (4) to the logarithmic regime yields A = 1 nm^2. We calculate ΔU using eqn (5) with z_C/r between 0 and 0.84 and find that the pinning energy is 5–10 kT. This value is low compared to the pinning energies found for aqueous-dispersed polymer spheres. The result is consistent with the notion that particles that reach a steady-state contact angles on experimental timescales pin the contact line with smaller energies.

Table 4 Fitted A and ΔU for various polymer particles. The uncertainties in ΔU account for uncertainties in the values of z_C and z_E

Particle type	A (nm^2)	ΔU (kT)
PMMA	7.1	55 ± 35
PVP-PMMA	6.3	50 ± 30
Sulfate-PS	4.6	55 ± 5
PVA-PS	11	100 ± 30

If we assume the surface asperities are roughly hemispherical caps, we can compare our fitted A directly with measurements of the roughness of silica spheres from Ruiz and coworkers,[45] who found the root-mean-squared roughness of 5.2 μm-diameter silica particles from Bangs Laboratories to be 1.4 nm using atomic force microscopy. The size we infer from our dynamic measurements is about 1 nm, in good agreement with the direct measurements.

We also examine 1 μm bare silica spheres approaching a water–decane interface from both phases. Most of the particles aggregate when we attempt to disperse them in decane. To obtain free particles, we discard the large aggregates that rapidly sediment and dilute the supernatant with more decane. We do not know whether the surface properties of silica in water and in decane are the same. However, we find that the smaller silica spheres reach a steady-state position within 20 ms when approaching from either phase, as shown in Fig. 7. We do not observe a logarithmic regime, and the spheres reach a steady-state height within the time resolution of our experiment. Because the interface in these experiments is not index-matched, the measured height is only approximate, so we do not calculate a contact angle.

The fast relaxation and absence of any observable logarithmic relaxation means that we cannot determine if transient pinning or viscous dissipation sets the rate of relaxation of these spheres. We can, however, interpret the results in the context of the dynamic models if we assume that the relaxation is determined by pinning. In that case, the absence of a logarithmic regime suggests either that the crossover between the fast and logarithmic relaxation regimes is at timescales longer than what we can observe or that the difference between z_E and z_C is small. According to eqn (5), a small difference between z_E and z_C means that $\Delta U/A$ is small. Indeed, atomic-force-microscope measurements of similar-sized silica spheres (0.74 μm-diameter particles from Duke) by Chen and coworkers[46] found the RMS roughness to be about 0.36 nm, which is smaller than the RMS roughness value for larger silica spheres (1.4 nm).[45] Thus one interpretation of our results is that the small asperities do pin the contact line, but with a smaller energy than the larger asperities seen on the large silica spheres, leading to a faster relaxation to equilibrium.

4.4 Logarithmic relaxation may occur even in sheared emulsion formation

Finally, we examine whether slow relaxation is an important effect to consider in the preparation of Pickering emulsion, which are usually made using vigorous mixing. For a 1.9 μm-diameter

§ Polystyrene with some PVA on the surface, angle taken from the measurement for ''double-cleaned'' polystyrene in Isa *et al.*[12]

¶ No measurements for the equilibrium contact angle of aqueous-dispersible PMMA particles could be found. The PMMA particles from Bangs Laboratories, Inc. are expected to be more hydrophilic than typical polystyrene particles.

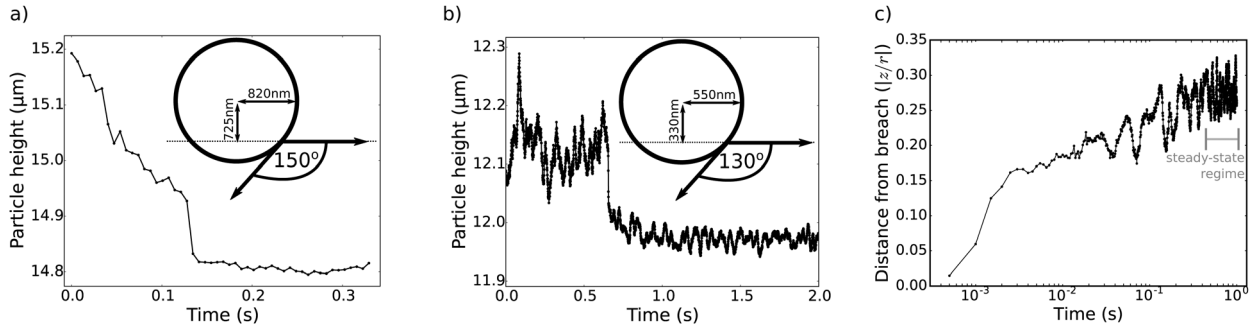

Fig. 6 (a) A PHSA-PMMA sphere reaches a steady-state contact angle of 150°. (b) Fluctuations of a 1.1 μm-diameter PDMS-PMMA particle decrease after the particle breaches the interface. The sphere reaches a steady-state contact angle of 130°. (c) The same data from (b) plotted on semilogarithmic axes, showing the initial logarithmic relaxation followed by the transition to a steady-state height.

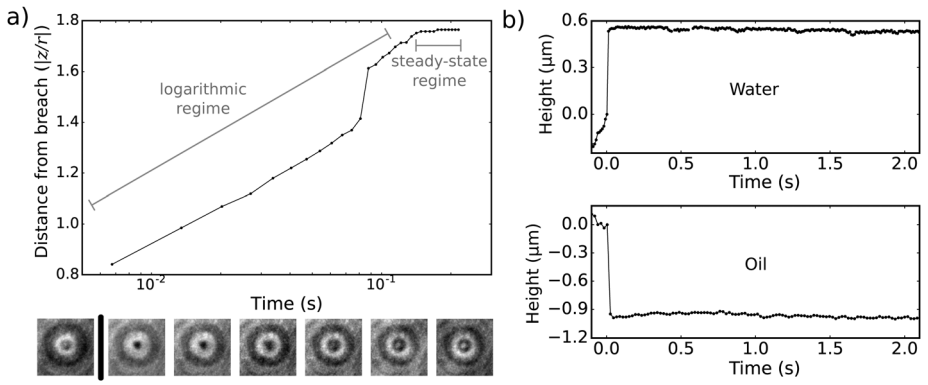

Fig. 7 (a) 4 μm silica spheres show logarithmic relaxation after breaching. The insets show holograms from 0.0068 s before, then 0.0068 s, 0.0136 s, 0.0271 s, 0.0542 s, 0.1084 s, and 0.2168 s after the breach. The central fringe slowly evolves from dark to bright, indicating a wavelength-scale change in the height of the particle. The jump at 0.8 s is a fast relaxation event, sometimes seen in our samples. (b) Trajectories of 1 μm silica spheres approaching the interface from the water (top) and decane (bottom) phases. In both cases, the particles rapidly reach a steady state height.

polystyrene sphere with an equilibrium contact angle of 110°, eqn (2) shows that the force on the particle integrated along the contact line is 10–100 nN for dynamic contact angles between 2° and 107°. The force on a 1.9 μm-diameter particle in a suspension that is mixed at 11 000 rpm in an Ultra Turrax homogenizer is about 1 nN,[47] orders of magnitude smaller than the capillary driving force. Thus the relaxation of the particles is unlikely to be hastened by mixing, and long equilibration times may be important to take into account in the preparation of Pickering emulsions. One way to determine the equilibration time is to vitrify emulsions at different times after formation and image the interfaces using a method similar to that of Coertjens *et al.*[12]

5 Discussion

We have shown that slow relaxation is common to many different kinds of particles, made of different materials and with different surface functionalities. Large silica particles and all of our polymer particles, whether stabilized in water or oil, relax to equilibrium at rates smaller than those expected from viscous dissipation alone. Thus we argue that the relaxation rate of colloidal particles at interfaces is likely controlled by transient pinning and unpinning of the three-phase contact line.

We have inferred certain features of the pinning sites by fitting dynamical models that account for pinning and depinning to our data. To gain further insight into the question of what surface features pin the contact line we now examine our results across the different types of systems. Our interpretation assumes that the dynamic models of Kaz *et al.* and Colosqui *et al.* capture the essential physics of the slow relaxation. Although there is little evidence that viscous dissipation controls the relaxation rate, we cannot—and do not attempt to—rule out the possibility that more complex wetting phenomena are responsible for the observed relaxation. Instead we focus on synthesizing a coherent explanation of the results in the context of the pinning models.

In all of the systems we observe, the area per defect is inferred to be on the order of a few square nanometers. This area is comparable to the area per charged group for aqueous charge-stabilized dispersions, as noted by Kaz *et al.*, but it is much smaller than the expected area per charged group for non-aqueous, sterically-stabilized polymer particles such as PHSA-PMMA. In the case of silica spheres, the area per defect is comparable to the measured surface roughness. We expect particles with more pronounced surface roughness to be affected more strongly by

contact-line pinning. Taken together, these results suggest that the pinning sites are small-scale topographical features, perhaps associated with anchored charged groups in aqueous charge-stabilized colloids, but not the charges themselves.

In all of the aqueous polymer dispersions, whether charge- or sterically stabilized, the inferred pinning energy per defect is approximately 50 kT. This value contrasts markedly with that of the sterically stabilized non-aqueous particles and silica spheres, which is only a few kT. To explain this difference we must consider how the surface of the aqueous polymer spheres differs from that of the non-aqueous polymer spheres and the silica.

One feature of aqueous polymer spheres that is sometimes mentioned in the literature is polymer ''hairs''; these are flexible polymer chains that are attached to the surface of the particles but extend out into solution and which may contain charged groups. The presence of such chains was originally inferred from electrophoretic mobility measurements: Rosen and Saville[38,48] found that both ''hairy'' polystyrene particles (with chains grafted onto their surface) and ''bare'' polystyrene particles had much lower electrophoretic mobilities than those predicted by classical electrokinetic theory. The discrepancy between experiment and theory was similar for both types of particles, suggesting that even ''bare'' particles have hairs. For both types of particles, the agreement between experiment and theory improved dramatically after the particles were heated past their glass transition temperature to allow the hairs to anneal to the surfaces of the particles. Further evidence for polymer hairs comes from optical measurements of the interaction between a polymer particle and a surface: Jensenius and Zocchi[49] found that some polystyrene particles attached to surfaces, and, by measuring the displacement of the particle, they concluded that the attachment tether was a single polymer chain with a coil size of 50 nm. These experiments suggest that polymer hairs may be a common feature of polymer particles, whether there are chains deliberately grafted onto the surface or not.

We therefore hypothesize that polymer hairs are the pinning sites on aqueous-dispersed polymer particles. Furthermore we hypothesize that the pinning sites on the non-aqueous polymer particles are also polymer hairs, which are likely the polymer stabilizers grafted onto the particles. A possible explanation for why the hairs on the non-aqueous particles have a much lower pinning energy than the hairs on the aqueous particles is that the ones on the aqueous particles are polyelectrolytes. Moving a polyelectrolyte from the aqueous to the oil phase may involve a large energy barrier because all of the charges need to first be neutralized. This explanation is not inconsistent with our results for how the pH affects the relaxation in carboxyl-PS spheres. In those experiments we found that changing the pH to be closer to the isoelectric point did not change the area per defect; if the defects are indeed polyelectrolyte hairs, we expect that some, but not all of the charges would be neutralized, and so the area per defect (per hair) would not change. However, the pinning energy should change with the pH. Therefore this hypothesis can be tested by observing how the crossover point between exponential and logarithmic relaxation changes as a function of pH, while independently measuring how the equilibrium contact angle changes with pH. This is a point for future experiments to examine. Measurements closer to the isoelectric point could also help to better isolate the effect of charge on breaching behavior.

6 Conclusions

The main message that emerges from our study is that slow, logarithmic relaxation is a common effect in colloidal particles bound to interfaces. By ''slow'' we mean slower than the rate expected from viscous dissipation alone. In many cases, however, the relaxation is slow even compared to experimental time scales. Our analysis of the forces involved suggests that the rate of relaxation will not be significantly altered by vigorous mixing; therefore experiments and applications (such as making Pickering emulsions) that involve attaching particles to interfaces and letting them assemble should account for the possibility that the particles are not in equilibrium on the timescale of assembly. We expect the out-of-equilibrium behavior to be most prominent in aqueous polymer particles a few hundred nanometers in diameter or larger; oil-dispersible polymer particles and silica spheres, even ones several micrometers in diameter, appear to equilibrate much more rapidly.

Based on the agreement between the observed logarithmic trajectories and the predictions of a model based on molecular kinetic theory, we have argued that the slow relaxation arises from surface heterogeneities that transiently pin the contact line. We ruled out the possibility that the heterogeneities are charged groups directly attached to the surfaces of the particles. Instead, the likely culprits for the pinning are topographical features—nanoscale surface roughness in the case of silica particles and polymer ''hairs'' in the case of polymer particles. Beyond the implications described above for the assembly of particles at interfaces, these results also show that the adsorption trajectory is a sensitive probe of nanoscale surface features that are difficult to measure directly.

Acknowledgements

We acknowledge support from the National Science Foundation through grant number DMR-1306410 and by the Harvard MRSEC through grant number DMR-1420570. We thank W. B. Rogers for his careful reading of this manuscript and suggestions; C. E. Colosqui, M. Mani and M. P. Brenner for critical discussions regarding the interpretation of these results and the model; A. Hollingsworth for providing the PHSA-stabilized PMMA particles and for helpful discussions about hairy particles; J. G. Park for providing the PVP-stabilized PMMA and PVA-stabilized polystyrene particles, and G. Meng for providing the PDMS-stabilized PMMA particles. The hologram analysis computations were run on the Odyssey cluster, supported by the FAS Science Division Research Computing Group at Harvard University. The zeta potential characterization was performed at the Center for Nanoscale Systems (CNS), a member of the National Nanotechnology Coordinated Infrastructure

Network (NNCI), which is supported by the National Science Foundation under NSF award no. 1541959. CNS is part of Harvard University.

References

1 S. U. Pickering, *J. Chem. Soc.*, 1907, **91**, 2001–2021.
2 M. Destribats, M. Rouvet, C. Gehin-Delval, C. Schmitt and B. P. Binks, *Soft Matter*, 2014, **10**, 6941–6954.
3 A. Timgren, M. Rayner, M. Sjöö and P. Dejmek, *Procedia Food Sci.*, 2011, **1**, 95–103.
4 T. Zhang, D. Davidson, S. L. Bryant and C. Huh, *et al.*, *SPE Improved Oil Recovery Symposium*, 2010.
5 D. Marku, M. Wahlgren, M. Rayner, M. Sjöö and A. Timgren, *Int. J. Pharm.*, 2012, **428**, 1–7.
6 A. Dinsmore, M. F. Hsu, M. Nikolaides, M. Marquez, A. Bausch and D. Weitz, *Science*, 2002, **298**, 1006–1009.
7 V. N. Paunov, *Langmuir*, 2003, **19**, 7970–7976.
8 M. Retsch, Z. Zhou, S. River, M. Kappl, X. S. Zhao, U. Jonas and Q. Li, *Macromol. Chem. Phys.*, 2009, **210**, 230–241.
9 L. Isa, K. Kumar, M. Müller, J. Grolig, M. Textor and E. Reimhult, *ACS Nano*, 2010, **4**, 5665–5670.
10 C. E. Colosqui, J. F. Morris and J. Koplik, *Phys. Rev. Lett.*, 2013, **111**, 028302.
11 D. M. Kaz, R. McGorty, M. Mani, M. P. Brenner and V. N. Manoharan, *Nat. Mater.*, 2012, **11**, 138–142.
12 S. Coertjens, P. Moldenaers, J. Vermant and L. Isa, *Langmuir*, 2014, **30**, 4289–4300.
13 G. Boniello, C. Blanc, D. Fedorenko, M. Medfai, N. B. Mbarek, M. In, M. Gross, A. Stocco and M. Nobili, *Nat. Mater.*, 2015, **14**, 908–911.
14 N. Sharifi-Mood, I. B. Liu and K. J. Stebe, *Soft Matter*, 2015, **11**, 6768–6779.
15 P. A. Kralchevsky, N. D. Denkov and K. D. Danov, *Langmuir*, 2001, **17**, 7694–7705.
16 R. McGorty, J. Fung, D. Kaz and V. N. Manoharan, *Mater. Today*, 2010, **13**, 34–42.
17 B. J. Park, J. Vermant and E. M. Furst, *Soft Matter*, 2010, **6**, 5327.
18 B. J. Park, J. P. Pantina, E. M. Furst, M. Oettel, S. Reynaert and J. Vermant, *Langmuir*, 2008, **24**, 1686–1694.
19 M. Nikolaides, A. Bausch, M. F. Hsu, A. Dinsmore, M. Brenner, C. Gay and D. Weitz, *Nature*, 2002, **420**, 299–301.
20 B. P. Binks, L. Isa and A. T. Tyowua, *Langmuir*, 2013, **29**, 4923–4927.
21 A. Wang, D. M. Kaz, R. McGorty and V. N. Manoharan, *AIP Conference Proceedings*, 2013, pp. 336–343.
22 T. D. Blake and J. M. Haynes, *J. Colloid Interface Sci.*, 1969, **30**, 421–423.
23 E. Rolley and C. Guthmann, *Phys. Rev. Lett.*, 2007, **98**, 166105.
24 J. H. Snoeijer and B. Andreotti, *Annu. Rev. Fluid Mech.*, 2013, **45**, 269–292.
25 H. Kramers, *Physica*, 1940, **7**, 284–304.
26 A. M. Rahmani, A. Wang, V. N. Manoharan and C. E. Colosqui, *Soft Matter*, 2016, **12**, 6365–6372.
27 A. J. Paine, W. Luymes and J. McNulty, *Macromolecules*, 1990, **23**, 3104–3109.
28 K. Cao, J. Yu, B.-G. Li, B.-F. Li and Z.-R. Pan, *Chem. Eng. J.*, 2000, **78**, 211–215.
29 S. M. Klein, V. N. Manoharan, D. J. Pine and F. F. Lange, *Colloid Polym. Sci.*, 2003, **282**, 7–13.
30 M. T. Elsesser and A. D. Hollingsworth, *Langmuir*, 2010, **26**, 17989–17996.
31 Y. Rotenberg, L. Boruvka and A. Neumann, *J. Colloid Interface Sci.*, 1983, **93**, 169–183.
32 Y. Touhami, G. H. Neale, V. Hornof and H. Khalfalah, *Colloids Surf., A*, 1996, **112**, 31–41.
33 J. Fung, R. W. Perry, T. G. Dimiduk and V. N. Manoharan, *J. Quant. Spectrosc. Radiat. Transfer*, 2012, **113**, 2482–2489.
34 B. Ovryn and S. H. Izen, *J. Opt. Soc. Am. A*, 2000, **17**, 1202–1213.
35 S. Lee, Y. Roichman, G. Yi, S. Kim, S. Yang, A. van Blaaderen, P. van Oostrum and D. G. Grier, *Opt. Express*, 2007, **15**, 18275–18282.
36 A. Egner and S. Hell, in *Handbook Of Biological Confocal Microscopy*, ed. J. B. Pawley, Springer US, 2006, pp. 404–413.
37 L. Rosen and D. Saville, *J. Colloid Interface Sci.*, 1990, **140**, 82–92.
38 L. Rosen and D. Saville, *J. Colloid Interface Sci.*, 1992, **149**, 542–552.
39 W. Chen, S. Tan, Z. Huang, T.-K. Ng, W. T. Ford and P. Tong, *Phys. Rev. E: Stat., Nonlinear, Soft Matter Phys.*, 2006, **74**, 021406.
40 B. J. Park and E. M. Furst, *Langmuir*, 2010, **26**, 10406–10410.
41 T. Tanaka, Y. Komatsu, T. Fujibayashi, H. Minami and M. Okubo, *Langmuir*, 2010, **26**, 3848–3853.
42 L. Isa, F. Lucas, R. Wepf and E. Reimhult, *Nat. Commun.*, 2011, **2**, 438.
43 A. Maestro, E. Guzmán, F. Ortega and R. G. Rubio, *Curr. Opin. Colloid Interface Sci.*, 2014, **19**, 355–367.
44 M. E. Leunissen, A. V. Blaaderen, A. D. Hollingsworth, M. T. Sullivan and P. M. Chaikin, *Proc. Natl. Acad. Sci. U. S. A.*, 2007, **104**, 2585–2590.
45 F. J. Montes Ruiz-Cabello, M. Moazzami-Gudarzi, M. Elzbieciak-Wodka, P. Maroni, C. Labbez, M. Borkovec and G. Trefalt, *Soft Matter*, 2015, **11**, 1562–1571.
46 W. Chen, S. Tan, Y. Zhou, T.-K. Ng, W. T. Ford and P. Tong, *Phys. Rev. E: Stat., Nonlinear, Soft Matter Phys.*, 2009, **79**, 041403.
47 H. Wang, V. Singh and S. H. Behrens, *J. Phys. Chem. Lett.*, 2012, **3**, 2986–2990.
48 D. Saville, *J. Colloid Interface Sci.*, 2000, **222**, 137–145.
49 H. Jensenius and G. Zocchi, *Phys. Rev. Lett.*, 1997, **79**, 5030.